

Numerical Procedure for Polycrystalline Ferroelectric/Ferroelastic Problems Using Landau's Phenomenological Model*

Gakuji NAGAI**, Takamasa HAYASHI** and Toshihisa TAKEKAWA***

**Department of Mathematical and Design Engineering, Gifu University,
Yanagido 1-1, Gifu, Gifu 501-1193, Japan
E-mail:gakuji@gifu-u.ac.jp

***Institute of Industrial Science, the University of Tokyo,
Komaba 4-6-1, Meguro-ku, Tokyo 153-8505, Japan

Abstract

This paper proposes a finite element procedure for the simulations of material nonlinearity so-called *domain switching* in polycrystalline ferroelectric/ferroelastic bodies. Conventional FEM, which has been used for linear piezoelectric analyses, is not appropriate for solving the nonlinear problem from thermodynamic viewpoint because it corresponds to finding a saddle point of functional. Therefore, we use a recently proposed alternative FEM that corresponds to finding local minimum points of functional. In the alternative FEM, both mechanical displacement and vector potential for electric displacement instead of scalar potential are chosen as unknown variables. As a constitutive law in each crystal, we adopt a class of Landau's potential energy models, which is a popular phenomenological description for phase transitions in solid-state physics. Because the processes of the nonlinear behavior are essentially dynamic phenomena and the total potential of the system may have local minimum solutions, we employ a dynamic formulation for the nonlinear analyses with the consideration of Debye-type dielectric relaxation and mechanical wave propagation. Numerical examples of a two-dimensional polycrystalline ferroelectric model are shown and the results can qualitatively predict ferroelectric behaviors such as hysteresis curves and butterfly curves.

Key words: Smart Materials, Thermodynamics, Domain Switching, Finite Element Method, Dynamic Analysis

1. Introduction

Ferroelectrics or *ferroelastics* is a coupling problem of electrostatics and mechanics and the term indicates the material nonlinearity so-called *domain switching* phenomena, which are related to phase transitions [1]. In the class of these materials, there are microscopically preferred directions of the spontaneous polarization that comes from crystal lattice structure, such as the tetragonal form of Perovskite structure below Curie temperature. The mechanism of domain switching is as follows; the preferred directions of spontaneous polarization suddenly change when electric or mechanical stimulations exceed certain thresholds. In addition most of the materials are polycrystalline and hence it makes their macroscopic responses more complicated.

For example, lead zirconium titanate (PZT) polycrystalline ceramics, which have been practically applied to electromechanical devices such as actuators and sensors, exhibit the

material nonlinearity when they are subjected to excessive electric or mechanical loads. Usually these applications are designed so that their responses are limited to be linear because the emergence of the nonlinearity means the degeneration of their functionalities. Another typical example is barium titanate (BaTiO_3). The functionality of this material is generally poorer than PZT but it is better for theoretical study because of its simple crystal lattice structure. One of the possible applications of these ferroelectric materials is non-volatile computer memory so-called *FeRAM* that utilizes their electric hysteresis loops due to the domain switching phenomena.

For the simulation of these linear responses, the finite element method (FEM) for electromechanical problem [2] has been widely used for several decades and many commercial finite element (FE) codes are available. In this conventional FEM, unknown variables are mechanical displacement \mathbf{u} and scalar potential ϕ well-known as electric voltage, and the obtained solutions correspond to a saddle point of functional.

On the other hand, for the simulation of material-nonlinear responses, there seems to be no widely accepted FE procedures and hence, as far as we know, no commercial FE codes are available. Its main difficulty would remain in nonlinear constitutive law. In solid-state physics, microscopic domain switching phenomena are often interpreted as the loss of quasi-stability in terms of thermodynamics. In addition, some constitutive models proposed for the conventional FEM exhibit numerical instabilities. Accordingly various approaches still have been studied for the numerical simulations of the material nonlinearity [3]. Furthermore, the conventional FEM would not be appropriate for the nonlinear simulations because it corresponds to finding a saddle point of functional. If some kinds of incomplete thermodynamic potentials are employed as constitutive models, it would be difficult for the conventional FEM to evaluate the constitutive laws for capturing quasi-stabilities.

In this paper, we propose a nonlinear numerical procedure for polycrystalline ferroelectric/ferroelastic problems. Hereafter, we refer to some kind of the averaged electromechanical behaviour of the polycrystalline materials as *macroscopic* behaviour and the constitutive behaviour of each single crystal grain as *microscopic* behaviour. As mentioned above, most engineering practical devices are usually in service within the linear range of their responses but it is still important both to understand and to predict their nonlinear responses because they may experience severe loads during their product life. In manufacturing process, it is essential to utilize microscopic domain switching phenomena in order to align the direction of their macroscopic polarization to the direction of applied excessive electric field [1]. Our attention is more paid to the development of a numerical procedure for understanding the domain switching phenomena in polycrystals. However, the developed methodology itself can be applied to the nonlinear analyses of practical devices with engineering-oriented constitutive models [4].

The procedure presented here is the combination of the following two components;

- (a) As a constitutive law in each crystal grain, a Landau's potential model is employed in conjunction with Debye-type dielectric relaxation effect [1]. Landau's models are popular phenomenological descriptions for phase transitions in solid-state physics and they can be also utilized for representing microscopic domain switching phenomena. In this class of models it is assumed that an incomplete thermodynamic potential A exists and it is a function of temperature T , strain $\boldsymbol{\varepsilon}$ and electric displacement \mathbf{D} . The free energy $A(T, \boldsymbol{\varepsilon}, \mathbf{D})$ has local minimums with respect to $\boldsymbol{\varepsilon}$ and \mathbf{D} , which are categorized into *extensive variables* or *generalized displacements*, and the number of local minimums depends on T . Note that work conjugates to the extensive variables are called *intensive variables* or *generalized forces*. Practically, $A(T, \boldsymbol{\varepsilon}, \mathbf{D})$ is expanded into the form of power series. Its local convexity corresponds to the states of quasi-stability and the loss of the local convexity, which is equivalent to the emergence of negative eigenvalues in its Hessian, corresponds to the onset of domain switching.

Since ferroelectric materials usually exhibit the time-dependent phenomena of dielectric relaxation, this dynamic effect is taken into account by introducing a simple Debye-type model.

- (b) To match the above Landau's constitutive law model, an alternative FEM [5], [6] is employed. This FEM has been recently proposed and unknown variables are both mechanical displacement \mathbf{u} and the vector potential $\boldsymbol{\psi}$ deriving \mathbf{D} instead of scalar potential ϕ . In terms of electrostatics, the alternative FEM and the conventional FEM are conjugate each other like force method versus displacement method in structural analyses, or nodal analysis versus closed-loop analysis in electric circuits. The alternative FEM is more advantageous than the conventional one in terms of thermodynamics because generally constitutive laws are single-valued functions with respect to the extensive variables $\boldsymbol{\varepsilon}$ and \mathbf{D} but their inverses tend to be multi-valued functions with respect to intensive variables, stress $\boldsymbol{\sigma}$ and electric field \mathbf{E} . The alternative FEM corresponds to finding local minimum points of functional. On the other hand, it has the restrictions; it is not guaranteed that vector potential $\boldsymbol{\psi}$ always exists and it is difficult to impose arbitrary electric conditions [6].

The resulting computational procedure is similar to that for the buckling analyses of structures like shallow arches. In this paper, after describing (a) and (b) in concrete form, we will show numerical examples of the constitutive law for BaTiO₃ and then demonstrate numerical examples of a two-dimensional polycrystalline ferroelectric model subjected to dynamic loadings.

2. Numerical procedure

2.1 Landau's potential model as constitutive law

Landau's potential model was originally proposed for the phenomenological descriptions of phase transitions. Since it can easily represent all primary features in simple expressions of power series, it is now widely accepted in solid-state physics whether it is true or not. One of the numerical applications is in the phase field methods [7]. Devonshire [8] has proposed a Landau's model for BaTiO₃. We employ an improved model of his as constitutive law to represent domain switching phenomena at certain constant temperature.

An incomplete thermodynamic potential A is assumed to exist and to be a function of temperature T , strain tensor $\boldsymbol{\varepsilon}$ and electric displacement tensor \mathbf{D} , i.e.,

$$A = A(T, \boldsymbol{\varepsilon}, \mathbf{D}) \quad (1)$$

Note that the variables in the function (1) except for T are often called *order parameters*, which can well represent the change of symmetric property in crystal lattice structure with the decrease of temperature T .

Stress tensor $\boldsymbol{\sigma}$ and electric field tensor \mathbf{E} are defined as

$$\boldsymbol{\sigma} \equiv \frac{\partial A}{\partial \boldsymbol{\varepsilon}}, \quad \mathbf{E} \equiv \frac{\partial A}{\partial \mathbf{D}} + \eta \dot{\mathbf{D}} \quad (2)$$

where the effect of dielectric relaxation has been taken into account by introducing a simple Debye-type model. η is a coefficient for this effect and $(\dot{})$ denotes a temporal differential operator. The second in Eq. (2) is analogous to Kelvin-Voigt model in viscoelasticity. The case of $\eta = 0$ stands for no dielectric relaxation and the second in Eq. (2) recovers an ordinal expression in thermodynamics.

In this paper, the following potential [9] is adopted.

$$A(T, \boldsymbol{\varepsilon}, \mathbf{D}) = G(T, \boldsymbol{\sigma}(\boldsymbol{\varepsilon}, \mathbf{D}), \mathbf{D}) + \boldsymbol{\sigma}(\boldsymbol{\varepsilon}, \mathbf{D}) : \boldsymbol{\varepsilon} \quad (3)$$

$$G = a_1 (D_1^2 + D_2^2 + D_3^2) + a_{11} (D_1^4 + D_2^4 + D_3^4)$$

$$\begin{aligned}
 &+ a_{12} (D_1^2 D_2^2 + D_2^2 D_3^2 + D_3^2 D_1^2) \\
 &+ a_{111} (D_1^6 + D_2^6 + D_3^6) \\
 &+ a_{112} (D_1^4 (D_2^2 + D_3^2) + D_2^4 (D_3^2 + D_1^2) + D_3^4 (D_1^2 + D_2^2)) \\
 &+ a_{123} D_1^2 D_2^2 D_3^2 \\
 &- (1/2) s_{11} (\sigma_{11}^2 + \sigma_{22}^2 + \sigma_{33}^2) \\
 &- s_{12} (\sigma_{11} \sigma_{22} + \sigma_{22} \sigma_{33} + \sigma_{33} \sigma_{11}) \\
 &- (1/2) s_{44} (\sigma_{23}^2 + \sigma_{31}^2 + \sigma_{12}^2) \\
 &- Q_{11} (\sigma_{11} D_1^2 + \sigma_{22} D_2^2 + \sigma_{33} D_3^2) \\
 &- Q_{12} (\sigma_{11} (D_2^2 + D_3^2) + \sigma_{22} (D_3^2 + D_1^2) + \sigma_{33} (D_1^2 + D_2^2)) \\
 &- Q_{44} (\sigma_{23} D_2 D_3 + \sigma_{31} D_3 D_1 + \sigma_{12} D_1 D_2)
 \end{aligned}$$

where a_1 , a_{11} and so on are coefficients. The above first equation is the Legendre transformation of the second one. Since the second one is convex upward with respect to σ , no information is lost due to the transformation. The coefficients for pure BaTiO₃ single crystal, which have been experimentally determined [9], are given as

$$\begin{aligned}
 a_1 &= 3.3 (T - 110) \times 10^5 \\
 a_{11} &= 3.6 (T - 175) \times 10^6 \\
 a_{12} &= 4.9 \times 10^8 \\
 a_{111} &= 6.6 \times 10^9 \\
 a_{112} &= 2.9 \times 10^9 \\
 a_{123} &= 7.6 (T - 120) \times 10^7 + 4.4 \times 10^{10} \\
 s_{11} &= 8.3 \times 10^{-12} \\
 s_{12} &= -2.7 \times 10^{-12} \\
 s_{44} &= 9.24 \times 10^{-12} \\
 Q_{11} &= 0.11 \\
 Q_{12} &= -0.043 \\
 Q_{44} &= 0.059
 \end{aligned} \tag{4}$$

where all the coefficients are in SI units and temperature T is in Celsius. It is obvious that for certain constant temperature the second equation in Eq. (2) is a single-valued function with respect to ε , D and \dot{D} while the partial inverse of it would become a multi-valued.

2.2 Alternative governing equations

After giving a form of governing equations, which has been used for the conventional FEM, we state an alternative and equivalent form for it. The alternative form matches the constitutive law described above. Because expected frequency is up to the order of MHz, mechanical wave propagation is taken into account while electrostatic approximation is still valid for dielectrics.

(a) Governing equation for conventional finite element formulation

Mechanical displacement \mathbf{u} and scalar potential ϕ are unknown variables in a body V . Differential equations for electromechanical problem are given by

$$\nabla \cdot \sigma + \mathbf{b} = \rho \ddot{\mathbf{u}}, \quad \sigma = \sigma(\varepsilon, E), \quad \varepsilon = \nabla^s \mathbf{u} \quad \text{in } V \tag{5}$$

$$\nabla \cdot D = q^v, \quad D = D(\varepsilon, E), \quad E = -\nabla \phi \quad \text{in } V \tag{6}$$

where \mathbf{b} , q^v and ρ are body force, volumetric charge density and mass density respectively, ∇ is a gradient operator, and the superscript s is an operator to take symmetric part. Each second equation of constitutive law in the above is just a symbolic expression for the ease of understanding.

Boundary conditions on the boundary S of the body V are given by

$$\mathbf{u} = \bar{\mathbf{u}} \quad \text{on } S^u, \quad \sigma \cdot \mathbf{n} = \mathbf{t} \quad \text{on } S^t \tag{7}$$

$$\phi = \bar{\phi} \quad \text{on } S^\phi, \quad D \cdot \mathbf{n} = q^s \quad \text{on } S^q \tag{8}$$

where $\bar{\mathbf{u}}$, $\bar{\phi}$, \mathbf{t} , and q^s are prescribed displacement, voltage, traction, and surface charge density, respectively, and \mathbf{n} is the outward unit normal vector of S . The displacement

boundary S^u and the traction boundary S^t are $S^u \cup S^t = S$ and $S^u \cap S^t = \emptyset$. Similarly, the electric voltage boundary S^ϕ and the surface charge boundary S^q are $S^\phi \cup S^q = S$ and $S^\phi \cap S^q = \emptyset$.

(b) Governing equation for present vector finite element formulation

Due to the vector calculus theorem, the third equation in Eq. (6) can be rewritten by using the following equivalence:

$$\exists \phi \text{ s. t. } \mathbf{E} = -\nabla \phi \Leftrightarrow \nabla \times \mathbf{E} = \mathbf{0} \quad (9)$$

If volumetric charge q^v can be restricted to zero, again due to the vector calculus theorem, the first equation in Eq. (6) can be rewritten by using the following equivalence:

$$\nabla \cdot \mathbf{D} = 0 \Leftrightarrow \exists \boldsymbol{\psi} \text{ s. t. } \mathbf{D} = \nabla \times \boldsymbol{\psi} \quad (10)$$

where $\boldsymbol{\psi}$ is a *vector potential* in three dimensions, which derives electric displacement \mathbf{D} . The restriction $q^v = 0$ is reasonable for many cases although it is severe for charged cases such as ion-doped materials. Note that because the vector potential $\boldsymbol{\psi}$ in three dimensions has the arbitrariness of scalar function a such that $\nabla \times \boldsymbol{\psi} = \nabla \times (\boldsymbol{\psi} + \nabla a)$, some kind of gauge fixing condition is required. Consequently, alternative differential equations to Eq. (5) and (6) are

$$\nabla \cdot \boldsymbol{\sigma} + \mathbf{b} = \rho \ddot{\mathbf{u}}, \quad \boldsymbol{\sigma} = \boldsymbol{\sigma}(\boldsymbol{\varepsilon}, \mathbf{D}), \quad \boldsymbol{\varepsilon} = \nabla^s \mathbf{u} \quad \text{in } V \quad (11)$$

$$\nabla \times \mathbf{E} = \mathbf{0}, \quad \mathbf{E} = \mathbf{E}(\boldsymbol{\varepsilon}, \mathbf{D}, \dot{\mathbf{D}}), \quad \mathbf{D} = \nabla \times \boldsymbol{\psi} \quad \text{in } V \quad (12)$$

where each second equation in the above corresponds to Eq. (2).

The electric boundary conditions can be also rewritten with the following two restrictions:

- (i) Surface charge density q^s must be zero on boundary S_{NL}^q , where $S_{NL}^q \subset S^q$. Namely, electric displacement \mathbf{D} does not leak across the boundary S_{NL}^q and hence, it is always parallel to S_{NL}^q . Note that $S^q \setminus S_{NL}^q$ is open electrodes, which are not subjected to prescribed voltages. The restriction $q^s = 0$ is trivial if surrounding environments such as the air are taken into account. In the strict sense, these environments could not be separated from ferroelectric bodies because it is physically hard to completely shield electrostatic field. In addition, the dielectric modulus is practically around 10^3 times as large as that of the air. For such a case, the restriction $q^s = 0$ is a reasonable approximation.
- (ii) Electric voltage ϕ on each connected electrode region S_{Ei} must be equipotential, where $\cup_i S_{Ei} = S^\phi \cup (S^q \setminus S_{NL}^q)$.

Let us begin by the transformation of the non-leakage boundary condition on S_{NL}^q . As illustrated in Fig. 1, the body V is virtually separated into two volumes by arbitrary section S_A so that the edge l_A of S_A does not cross any electrodes S_{Ei} . Unless the section S_A steps over them, total electric charge Q leaked across the one side of S_A does not vary,

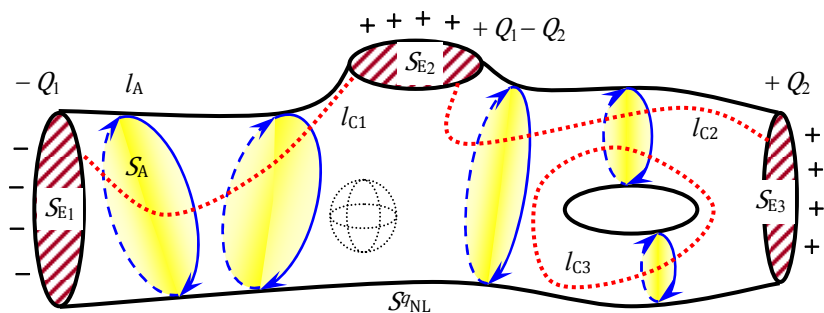


Fig. 1 Electric boundary conditions for vector potential

i.e.,

$$Q = \int_{S_A} \mathbf{D} \cdot \mathbf{n}_A dS = (\text{Piecewise constant}) \quad (13)$$

where \mathbf{n}_A is the outward unit normal vector of S_A of an interesting volume side. Substituting the third equation in Eq. (12) into the above equation and applying Stokes' theorem to it yields

$$\begin{aligned} Q &= \int_{S_A} (\nabla \times \boldsymbol{\psi}) \cdot \mathbf{n}_A dS \\ &= \oint_{l_A} \boldsymbol{\psi} \cdot \mathbf{t}_A dl = (\text{Piecewise constant}) \quad \text{for } \forall l_A \subset S_{NL}^q \end{aligned} \quad (14)$$

where \mathbf{t}_A is the unit tangential vector of closed-loop l_A whose direction is counterclockwise when it is viewed from the outside of the interesting volume.

Next, thanks to the restriction of equipotential voltage on each electrode S_{Ei} , electric field \mathbf{E} on boundary surface S_{Ei} is perpendicular to the S_{Ei} , i.e.,

$$\mathbf{E} \times \mathbf{n} = \mathbf{0} \quad \text{on } \cup_i S_{Ei} \quad (15)$$

However, this condition has missed information about voltage. To recover it, the following definition of the voltage of difference is applied whenever it is required.

$$\Delta\phi_j \equiv - \int_{l_{Cj}} \mathbf{E} \cdot \mathbf{t}_{Cj} dl \quad (16)$$

where as illustrated in Fig. 1, l_{Cj} is the j -th arbitrary path that connects two different electrodes in $\cup_i S_{Ei}$ in V or on S , \mathbf{t}_{Cj} is the unit tangent vector of l_{Cj} , and $\Delta\phi_j$ is the voltage of difference whose reference point is the electrode from which \mathbf{t}_{Cj} departs. If a hole exists in V , l_{Cj} is the path that goes around the hole and $\Delta\phi_j = 0$, which means that a virtual electrode is introduced and the path returns to itself. Consequently, alternative electric boundary conditions to Eq. (8) are Eqs. (14), (15), and (16). Mechanical boundary condition Eq. (7) is not changed.

2.3 Weak form

Introducing weight functions $\delta\mathbf{u}$ and $\delta\boldsymbol{\psi}$ and taking weighted residuals for the first in Eq. (11) and the second in Eq. (7), and for the first in Eq. (12) and Eq. (15), we have

$$\int_V \delta\mathbf{u} \cdot (\nabla \cdot \boldsymbol{\sigma} + \mathbf{b} - \rho\ddot{\mathbf{u}}) dV + \int_{S^t} \delta\mathbf{u} \cdot (\mathbf{t} - \boldsymbol{\sigma} \cdot \mathbf{n}) dS = 0 \quad (17)$$

$$\int_V \delta\boldsymbol{\psi} \cdot (\nabla \times \mathbf{E}) dV + \int_{\cup_i S_{Ei}} \delta\boldsymbol{\psi} \cdot (\mathbf{E} \times \mathbf{n}) dS = 0 \quad (18)$$

where $\delta\mathbf{u} = \mathbf{0}$ on S^u and $\delta Q \equiv \oint_{l_A} \delta\boldsymbol{\psi} \cdot \mathbf{t}_A dl = (\text{Piecewise constant})$ for $\forall l_A \subset S_{NL}^q$. Applying Gauss' divergence theorem to Eq. (17) yields

$$\int_V \rho \delta\mathbf{u} \cdot \ddot{\mathbf{u}} dV + \int_V \delta\boldsymbol{\varepsilon} : \boldsymbol{\sigma} dV - \int_V \delta\mathbf{u} \cdot \mathbf{b} dV - \int_{S^t} \delta\mathbf{u} \cdot \mathbf{t} dS = 0 \quad (19)$$

where $\delta\boldsymbol{\varepsilon} = \nabla^s \delta\mathbf{u}$. For Eq. (18), the formula, $\nabla \cdot (\delta\boldsymbol{\psi} \times \mathbf{E}) = (\nabla \times \delta\boldsymbol{\psi}) \cdot \mathbf{E} - \delta\boldsymbol{\psi} \cdot (\nabla \times \mathbf{E})$, Gauss' divergence theorem and the formula for scalar triple product, $(\delta\boldsymbol{\psi} \times \mathbf{E}) \cdot \mathbf{n} = \delta\boldsymbol{\psi} \cdot (\mathbf{E} \times \mathbf{n}) = -\mathbf{E} \cdot (\delta\boldsymbol{\psi} \times \mathbf{n})$ gives

$$\int_V \delta\mathbf{D} \cdot \mathbf{E} dV + \int_{S \setminus \cup_i S_{Ei}} \mathbf{E} \cdot (\delta\boldsymbol{\psi} \times \mathbf{n}) dS = 0 \quad (20)$$

where $\delta\mathbf{D} = \nabla \times \delta\boldsymbol{\psi}$.

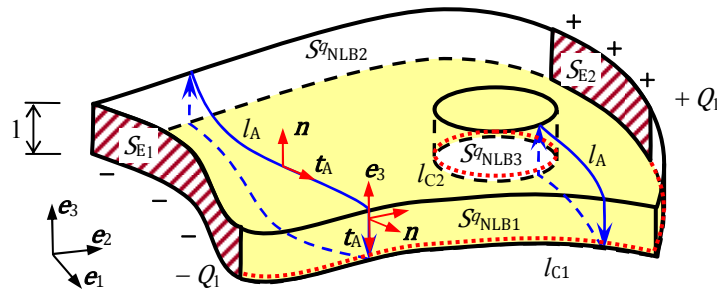


Fig. 2 Unit-thickness slab for 2-D case

For two-dimensional case, a slab model of unit thickness in x_3 direction, as illustrated in Fig. 2, is considered and $\boldsymbol{\psi} = \psi_3 \mathbf{e}_3$ and $\delta \boldsymbol{\psi} = \delta \psi_3 \mathbf{e}_3$ are assumed, where \mathbf{e}_3 is a unit vector in positive x_3 direction. The scalar field ψ_3 is known as *stream function*. In this case, Eq. (14) is simplified to

$$(\text{Piecewise constant}) = Q = \oint_{l_A} \psi_3 \mathbf{e}_3 \cdot \mathbf{t}_A dl = \psi_3|_{\text{back side}} - \psi_3|_{\text{front side}} \quad (21)$$

Therefore, stream function ψ_3 must keep the same value along each non-leakage side of the slab, which is well-known. Because $\mathbf{e}_3 \times \mathbf{n}$ is zero on the upper and the lower faces of the slab, and it is a unit tangential vector along the j -th non-leakage side of the slab, S^q_{NLBj} , Eq. (20) becomes

$$\int_V \delta \mathbf{D} \cdot \mathbf{E} dV - \sum_j \int_{S^q_{NLBj}} \delta \psi_3 \mathbf{E} \cdot (\mathbf{e}_3 \times \mathbf{n}) dS = 0 \quad (22)$$

Taking into account of Eq. (16), we have

$$\int_V \delta \mathbf{D} \cdot \mathbf{E} dV + \sum_j \delta Q_j \Delta \phi_j = 0 \quad (23)$$

Note that in two dimensions, ψ_3 is discretized by ordinal nodal finite elements and no gauge fixing condition is required, but in three dimensions, vector potential field $\boldsymbol{\psi}$ should be discretized not by nodal finite elements but by edge finite elements [6]. From the viewpoint of implementation, Eq. (21) is imposed by dependent degrees of freedom on non-leakage boundaries and one of these degrees is fixed to be zero, which corresponds to a sufficient condition for this problem.

2.4 Semi-discretized equations

The space discretization of Eq. (19) and (23) by finite element method results in the following nonlinear semi-discretized equations:

$$\begin{bmatrix} \mathbf{M}_M & \mathbf{0} \\ \mathbf{0} & \mathbf{0} \end{bmatrix} \begin{Bmatrix} \ddot{\mathbf{U}} \\ \ddot{\boldsymbol{\Psi}} \end{Bmatrix} + \begin{bmatrix} \mathbf{0} & \mathbf{0} \\ \mathbf{0} & \mathbf{C}_E \end{bmatrix} \begin{Bmatrix} \dot{\mathbf{U}} \\ \dot{\boldsymbol{\Psi}} \end{Bmatrix} + \begin{Bmatrix} \mathbf{f}_M^{\text{In Static}}(\mathbf{U}, \boldsymbol{\Psi}) \\ \mathbf{f}_E^{\text{In Static}}(\mathbf{U}, \boldsymbol{\Psi}) \end{Bmatrix} = \begin{Bmatrix} \mathbf{f}_M^{\text{Ex}} \\ \mathbf{f}_E^{\text{Ex}} \end{Bmatrix} \quad (23)$$

where \mathbf{U} and $\boldsymbol{\Psi}$ are a column vector of nodal displacements and a column vector of nodal stream functions in two dimensions (or a column vector of the line integrations of projected vector potential to the corresponding element edge in three dimensions), respectively, \mathbf{f}_M^{Ex} and \mathbf{f}_E^{Ex} are time-dependent external loads, and the other variables are derived in usual FEM contexts. Equation (23) is solved by using the Newmark β method ($\gamma = 1/2$, $\beta = 1/4$), which is unconditionally stable for linear cases, and the Newton-Raphson method.

3. Numerical examples in two dimensions

To show the basic applicability of the present procedure to polycrystalline

ferroelectric/ferroelastic problems, we focus on two dimensional cases of pure BaTiO₃ polycrystals. Hereafter $\rho = 5300$ in SI units and $T = 23$ in Celsius are used and by preliminary analyses $\eta = 10$ in SI units is assumed.

3.1 Verification of constitutive law

The constitutive law (2), (3) and (4) is reduced to two dimensions by letting $D_3 = \varepsilon_{33} = \varepsilon_{23} = \varepsilon_{31} = 0$ and its principal axes are aligned to global axes. The reduced system is solved by the backward Euler method with time increment $\Delta t = 0.5 \times 10^{-8}$ sec. The following results are interpreted as microscopic behaviors in a single crystal grain.

The first examples are the cases of pure uni-axial electric loading without mechanical stress. Three types of triangular wave of electric field with 30kV/mm in magnitude are applied in x_2 direction. They are 10kHz, 100kHz and 1MHz in frequency. Figure 3 plots the relations of electric field E_2 and electric displacement D_2 , and the relation of electric field E_2 and strain ε_{22} . They can represent physically-observed hysteresis curves in E_2 - D_2 and butterfly curves in E_2 - ε_{22} . It is obvious from the figures that the relations are strongly influenced by frequency due to the simple Debye-type model of Eq. (2). In the 1MHz response, D_2 can not follow the E_2 fluctuation.

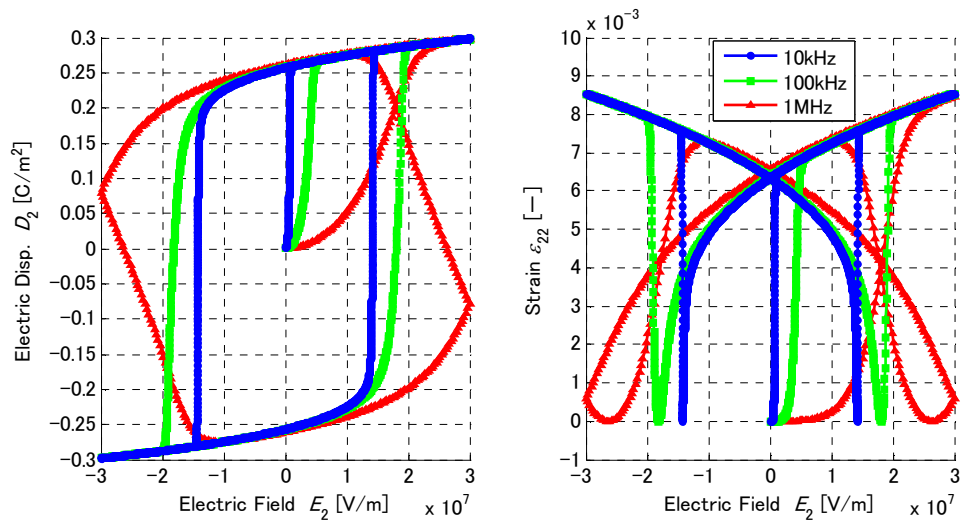


Fig. 3 Constitutive relations for uni-axial electric load

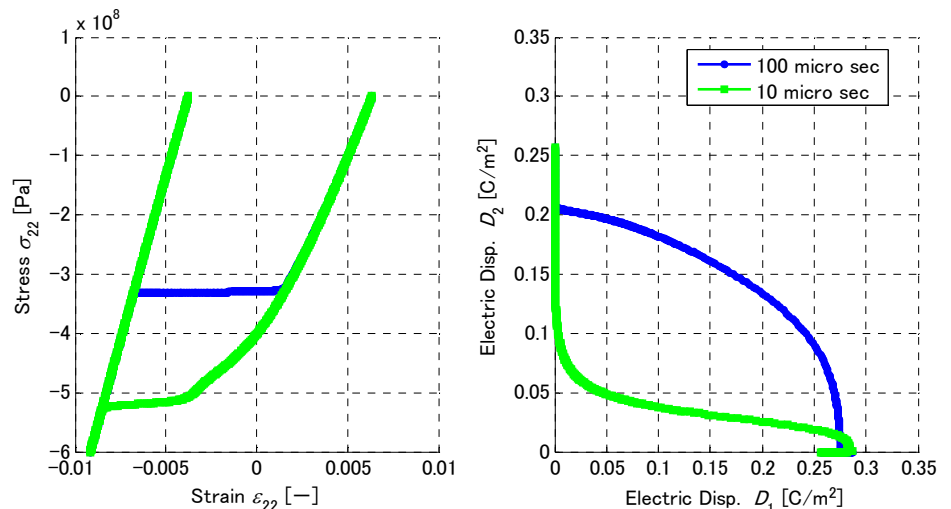


Fig. 4 Constitutive relations for uni-axial mechanical compression

The second examples are the cases of pure uni-axial mechanical loading without electric field. Initially electric displacement (spontaneous polarization) in the infinitesimal body is aligned to global x_2 direction. Two types of one triangular wave of compressive stress with 600MPa in magnitude are applied in x_2 direction. They are 100 μ sec and 10 μ sec in duration time. Figure 4 plots the relations of strain ε_{22} and stress σ_{22} , and the relation of D_1 and D_2 .

3.2 Polycrystalline model

Figure 5 shows a two-dimensional finite element mesh of polycrystalline model in electromechanically plain strain condition. Each single crystal grain has different local principal axes that are randomly defined. Along the interfaces between the grains, the continuity conditions of surface charge density and surface traction are automatically satisfied due to the governing equation. The sectional area is a square of 100 μ m length and electrodes are attached on both lower and upper faces. The both faces are mechanically constrained by horizontal rollers. The loading histories applied to the both faces are, in terms of average, the same as the ones described above.

For the electric loadings, the macroscopic results plotted in Fig. 6 that are the averaged gradient of differences between upper and lower faces are obtained. It is observed that macroscopic coercive electric field at 10kHz is as small as about half of the microscopic one of the constitutive law in Fig. 3 but the macroscopic one at 1MHz is very similar to the microscopic one. Dynamic effect relatively strongly appears in the macroscopic coercive electric field at 100kHz, compared to the microscopic one. All macroscopic strains ε_{22} are about two thirds of the microscopic ones. This is due to electromechanical interlocking among grains. Figure 7 shows the sequential processes of domain switching. All deformed

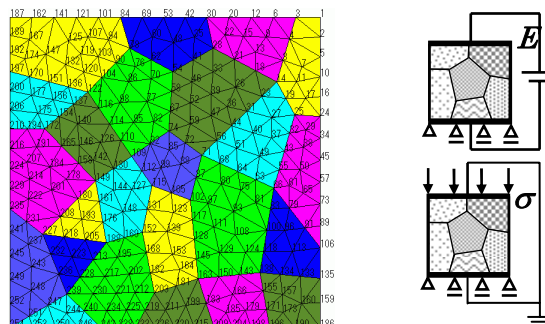


Fig. 5 Finite element mesh of polycrystalline model and boundary conditions

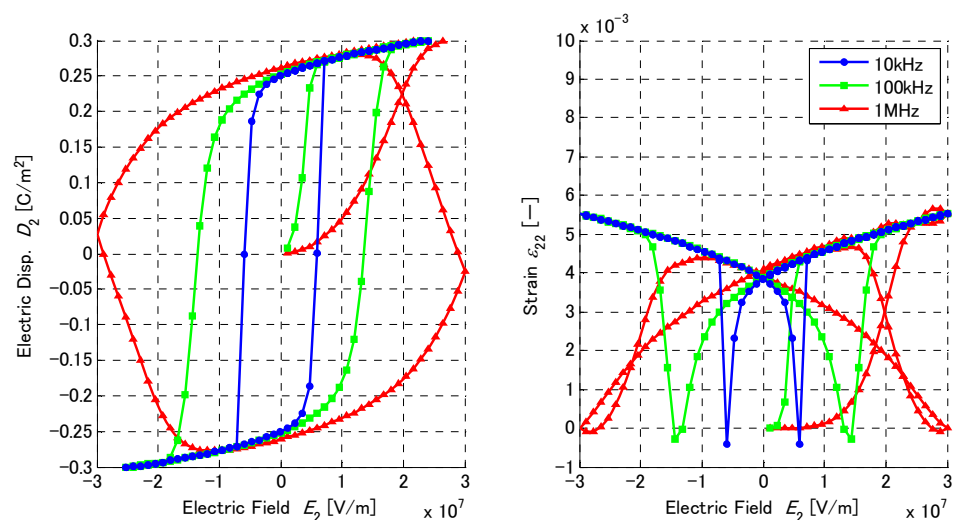


Fig. 6 Macroscopic relations for uni-axial electric load

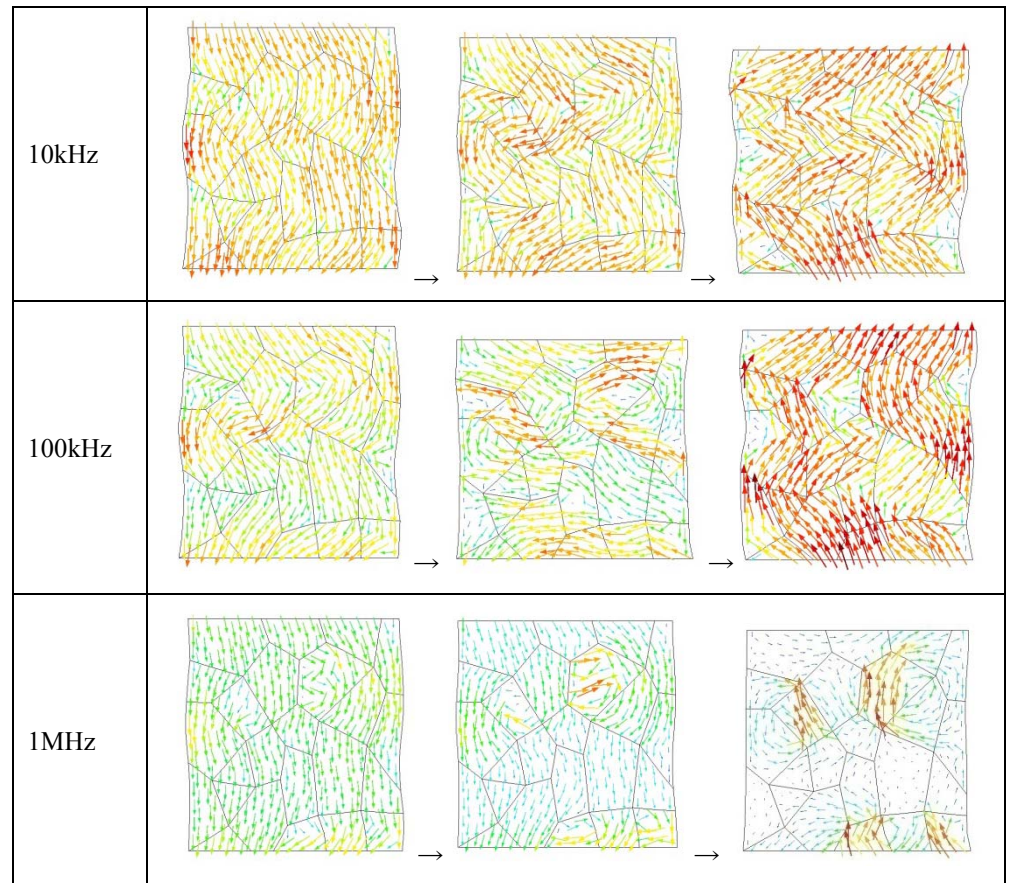


Fig. 7 Processes of domain switching

shapes are scaled by the same factor and the arrows indicates electric displacement \mathbf{D} . The distributions of electric displacement in 10kHz and 100kHz cases are similar and the flows of the fluxes tend to be elongate due to no volumetric charge, Eq. (10). On the other hand, 1MHz case is quite different. In electric displacement field, higher frequency leads to more local vortices and less intensity during domain switching process.

For the mechanical loadings of uni-axial compressive stress in x_2 direction, the macroscopic results in Fig. 8 are obtained. In advance of the mechanical loadings, electric displacements in the body are macroscopically aligned to x_2 direction by applying excessive electric field. Compared to the clear coercive stresses of microscopic constitutive law in Fig. 4, it becomes difficult to determine the linear limits due to the heterogeneity of polycrystals. Macroscopic depolarization after unloadings can be also seen. Figure 9 shows the processes of 100μsec case. The distribution of electric displacement in the right figure is the final status after unloading. The little macroscopic polarization at the final is due to the circuit shortcut between upper and lower electrodes.

4. Concluding remarks

A dynamic nonlinear finite element procedure for polycrystalline ferroelectric/ferroelastic problems has been proposed. Alternative FEM that is conjugate to the conventional FEM in terms of electrostatics has been introduced to be consistent with the class of the constitutive laws derived from Landau's potential models. Two dimensional numerical examples show that the present procedure can predict qualitatively their nonlinear responses so-called domain switching phenomena with the consideration of their heterogeneities. In the future work, constitutive laws, especially the modeling of dielectric relaxation, should be improved.

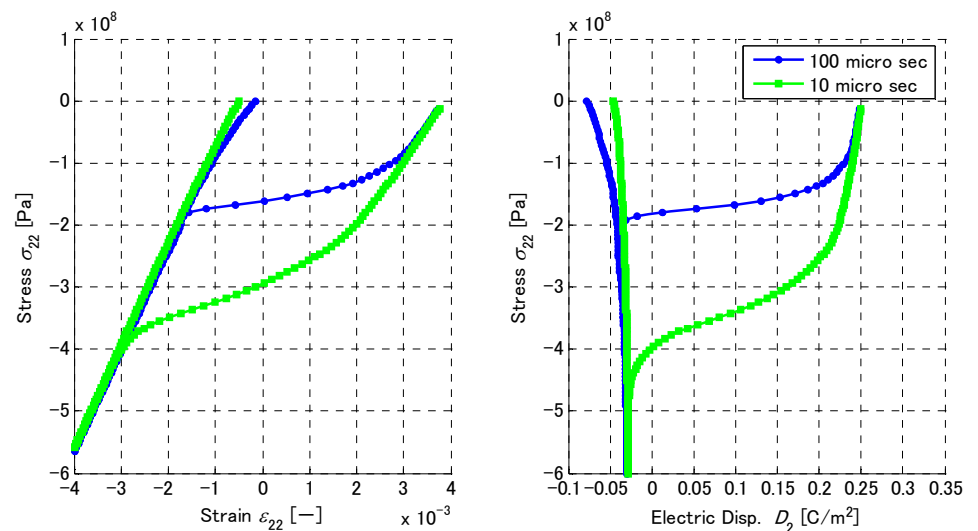


Fig. 8 Macroscopic relations for uni-axial compressive load

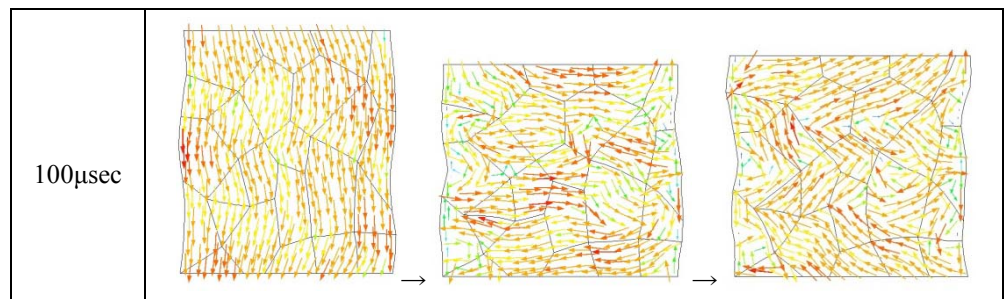


Fig. 9 Processes of macroscopic compressive load

Acknowledgements

This work was supported by Grants-in-Aid for Scientific Research (18760062).

References

- [1] J. Moulson and J. M. Herbert, *Electroceramics* second edition, *Wiley*, 2003
- [2] H. Allik and T. J. R. Hughes, Finite element method for piezoelectric vibration, *International Journal for Numerical Methods in Engineering*, 2, (1970), pp. 151-157
- [3] M. Kamlah, Ferroelectric and ferroelastic piezoceramics – modeling of electromechanical hysteresis phenomena, *Continuum Mechanics and Thermodynamics*, 13, (2001), pp. 219-268
- [4] J. E. Huber, N. A. Fleck, C. M. Landis and R. M. McMeeking, A constitutive model for ferroelectric polycrystals, *Journal of the mechanics and physics of solids*, 44, (1999), pp. 1663-1697
- [5] C. M. Landis, A new finite-element formulation for electromechanical boundary value problems, *Int. J. Num. Meth. Eng.*, 55, (2002), pp. 613-628
- [6] G. Nagai, T. Hayashi and K. Umemura, Three-dimensional vector finite element for ferroelectric/ferroelastic problem, *Proceedings of APCOM'07-EPMESE XI*, Kyoto, Japan (2007), in CD-ROM
- [7] L. Q. Chen, Models for microstructure evolution, *Annual Review of Materials Research*, 32, (2002), pp. 113-140
- [8] A. F. Devonshire, Theory of ferroelectrics, *Advances in physics*, 3, (1954), pp. 85-130
- [9] N. A. Pertsev, A. G. Zembilgotov and A. K. Tagantsev, Effect of mechanical boundary conditions on phase diagrams of epitaxial ferroelectric thin films, *Physical review letters*, 80(9), (1998), pp. 1988-1991